J Mol Model (2013) 19:879–891
DOI 10.1007/s00894-012-1620-z

ORIGINAL PAPER

Molecular dynamics and QM/MM-based 3D interaction analyses of cyclin-E inhibitors

Farhan Ahmad Pasha · Mohammad Morshed Neaz

Received: 28 July 2011 / Accepted: 30 September 2012 / Published online: 20 October 2012

Abstract Abnormal expression of cyclin-dependent kinase 2 (CDK2)/cyclin-E is detected in colorectal, ovarian, breast and prostate cancers. The study of CDK2 with a bound inhibitor revealed CDK2 as a potential therapeutic target for several proliferative diseases. Several highly selective inhibitors of CDK2 are currently undergoing clinical trials, but possibilities remain for the identification and development of novel and improved inhibitors. For example, in silico targeting of ATP-competitive inhibitors of CDKs is of special interest. A series of 3,5-diaminoindazoles was studied using molecular docking and comparative field analyses. We used post-docking short time molecular dynamics (MD) simulation to account for receptor flexibility. The three types of structures, i.e., the highest energy, lowest energy and the structure most resembling the X-ray structure (three complexes) were identified for all ligands. QM/MM energy calculations were performed using a DFT b3lyp/6–31 g* and MM OPLS-2005 force field. Conceptual DFT properties such as the interaction energy of ligand to protein, global hardness (η), HOMO density, electrostatic potential, and electron density were calculated and related to inhibitory activity. CoMFA and CoMSIA were used to account for steric and electrostatic interactions. The results of this study provide insight into the bioactive conformation, interactions involved, and the effect of different drug fragments over different biological activities.

F. A. Pasha (✉)
Applied Chemistry and Physical Chemistry Division,
Institut Français du Pétrole (IFP),
1 et 4 rue Bois Préau,
92582 Rueil Malmaison, France
e-mail: fpasha@rediffmail.com

F. A. Pasha · M. M. Neaz
Korea Institute of Science and Technology,
PO Box 131, Seoul 130-650, South Korea

Keywords Drug design · CDK2 · Kinase · QM/MM · MD

Introduction

The cyclin-dependent kinases (CDKs) are a family of serine-threonine protein kinases that govern the initiation, progression, and completion of the cell cycle. These kinases are responsible for controlling cell cycle progression, operating at the transition from G2 to M and G1 to S phases. Progression through S phase is regulated by a complex set of mechanisms, including the presence of activating cyclins, regulatory phosphorylation and endogenous CDK inhibitors at checkpoints [1]. Individual CDKs can phosphorylate distinct substrates at different phases of the cell cycle so they have been classified as G1 (CDK4 and CDK6-D cyclins, CDK2- cyclin E), S (CDK2-cyclin A, CDK1-cyclin A), and G2/M (CDK1-cyclin B) phase-specific CDKs. The assembly of a CDK with its corresponding cyclin yields a partially active complex. Full activity is achieved after phosphorylation of the CDK at the conserved threonine residue proximal to the ATP-binding cleft (Thr 172 in CDK4/6, Thr 160 in CDK2, and Thr 161 in Cdc2) [2–7]. Assembly of the cyclin leads to conformational changes in the T-loop, making it more accessible for phosphorylation. Phosphorylation causes a further conformational change in the T-loop, making the catalytic cleft fully accessible to ATP. In addition to the kinase activity, phosphorylation is also known to enhance the stability of some cyclin/CDs [7–9]. CDK2 complexes with cyclin E and A are required for S phase (DNA synthesis) progression of the cell cycle [10–16].

CDK inhibitors decrease the kinase activity of the cyclin/CDK complex by blocking the transition from G1 to S phase [17]. A study of the active site of CDK2 with a bound inhibitor showed CDK2 to act as a potential therapeutic

target for cancer [18]. Inhibitors with a high selectivity for CDK2, such as roscovitine/CYC-202 [19] and BMS-387032/SNS-032 [19], are currently undergoing phase I and II clinical trials.

Here, in order to understand the conformational compatibility of novel ligands with their receptor, we used in silico molecular dynamic (MD) simulations. Charge perturbation and energy exchange within the complex were analyzed using density functional theory (DFT) [20]. Computational time was reduced using a hybrid QM/MM [21, 22] method in which the ligand was defined by DFT (b3lyp/6–31g*) while the rest of the protein and the solvent molecules were defined using molecular mechanics (OPLS force field) [23]. The conceptual DFT properties yielded promising results for molecular recognition [24–27]; consequently, we used DFT properties such as interaction energy, global hardness (η) and frontier orbital energies to correlate with variations in inhibitory activity for a series of compounds. The molecular fields and molecular similarity effects on biological activity were also considered using CoMFA/CoMSIA [28–30].

Materials and methods

Dataset

A series of 3,5-diaminoindazoles known to have CDK inhibitory activities [31] were considered for this study. The in vitro CDK inhibitory activities were converted into corresponding pIC_{50} ($-\log IC_{50}$) values. The set of 28 CDK inhibitors was divided into a training set (22 compounds) and a test set (6 compounds) as reported in Table 1. Selection of the molecules for the training and test sets was based on the fact that test set molecules must have a range of biological activity and typical chemical structures similar to those of the training set.

Construction

The bioactive conformation of the most active molecule (compound **14**) was docked using Glide [32]. The docked conformer was used as template to construct 3D models of all other molecules using the maestro interface [33]. Minimum energy conformers were obtained using random search algorithms and further minimized using OPLS force field with a distance-dependent dielectric and the Powell conjugate gradient algorithm. The convergence criterion was 0.05 kcal mol^{-1} $Å^{-1}$. The partial atomic charges were assigned using OPLS force field.

Molecular docking

All inhibitors were minimized using the OPLS-2005 force field using Macro Model [23]. The crystal structure of CDK2 (PDB 1YKR) was used as the receptor for this study [34]. The Glide molecular docking program was used for docking and calculation of binding affinities. During the docking process, Glide performs an initial complete systematic search for conformational, orientational and positional space for the docked ligand and eliminates unwanted conformations using scoring, followed by energy minimization. Details of the algorithm are available in the GLIDE documentation. Briefly, GLIDE proprietary conformational expansion and exhaustive search of the binding site produce a multitude of ligand poses, which undergo an initial refinement, energy minimization on a pre-computed grid, and a final scoring and ranking. GLIDE uses proprietary scoring functions that are variations of the Chem Score 43 empirical scoring function and the OPLS-2005 force field to compute van der Waals and electrostatic grids for the receptor. The final ligand binding poses were ranked according to a computed Emodel score that encompasses the grid score, the proprietary Glide score, and the internal energy strain. The inhibitors were docked into the receptor site using GLIDE SP (standard precision) mode.

Pose selections

A total of 100 docked conformers for each ligand was reported. The best pose for each ligand was selected using the docked score and the total energy as a first criterion, while similarity and orientation to the co-crystallized ligand (Fig. 1) was used as a secondary criterion.

Molecular dynamics

The best-docked pose for each ligand was solvated using a water box [simple point charge (SPC)] of 55 Å (Fig. 2). The ligand and residues in the surrounding 5 Å (namely Glu8, Lys9, Ile10, Gly11, Glu12, Gly13, Lys20, Val 64, Phe80, Glu81, Phe82, Leu83, His84, Gln85, Asp86, Lys129, Pro130, Gln131, Asn132, Ala144, and Asp145) were allowed to move while other residues and water molecules were kept frozen. A short term 10 ns MD simulation was performed using Macro model as implemented in the Schrödinger suite [33] .

The MD run was performed using OPLS2005 potential with force field based charges and PRCG algorithms. The maximum 500 iterations were considered with gradient convergence criterion and a convergence threshold of 0.05. Non-bonded cutoff values of 8 Å for van der Waals interaction and 20 Å for the electrostatic interaction were set for

Table 1 Structures of diaminoindazole-based cyclin-dependent kinase 2 (CDK2) inhibitors with their observed activities. *MITZDO* 2-Methyl-isothiazolidine-1,1-dioxide

No.	R1	R2	IC_{50} (μM)	pIC_{50}
1	Phenyl-	NO_2	2.000	5.70
2	Phenyl-	C_2H_5NH	0.500	6.30
3	Phenyl-	$(C_2H_5)_2N$	0.200	6.70
4	Phenyl-	$(n\text{-}C_3H_7)_2N$	1.800	5.74
5	Phenyl-	$CO(CH_2)_3N$	0.170	6.77
6	Phenyl-	$CO(CH_2)_4N$	7.100	5.15
7	Phenyl-	$COCH_2NHCON$	2.000	5.70
8	Phenyl-	$SO_2(CH_2)_3N$	0.040	7.44
9	3-F-C_6H_4-	MITZDO	0.010	8.00
10	4-F-C_6H_4-	MITZDO	0.020	7.70
11	2-Cl-C_6H_4-	MITZDO	0.024	7.62
12	3-Cl-C_6H_4-	MITZDO	0.010	8.00
13	4-Cl-C_6H_4-	MITZDO	0.010	8.00
14	3-Br-C_6H_4-	MITZDO	0.007	8.15
15	4-Br-C_6H_4-	MITZDO	0.007	8.15
16	3-CH_3-C_6H_4-	MITZDO	0.010	8.00
17	4-CH_3-C_6H_4-	MITZDO	0.007	8.15
18	4-HO-C_6H_4-	MITZDO	0.009	8.05
19	4-NH_2-C_6H_4-	MITZDO	0.016	7.80
20	4-$(CH_3)_2$N-C_6H_4-	MITZDO	0.010	8.00
21	4-(C2H5)2 N-C_6H_4-	MITZDO	0.040	7.40
22	4-(1-Piperidinyl)-C_6H_4-	MITZDO	0.030	7.52
23	4-CH_3S-C_6H_4-	MITZDO	0.010	8.00
24	4-CH_3SO_2-C_6H_4-	MITZDO	0.022	7.66
25	1-Naphthyl	MITZDO	0.020	7.70
26	2-Naphthyl	MITZDO	0.009	8.05
27	4-Biphenyl-	MITZDO	0.014	7.85
28	4-(4-Pyridyl)-C_6H_4-	MITZDO	0.030	7.52

formally charged atoms. All bonds were allowed to SHAKE and the simulation temperature was 310 K with a 1.5-fs time steps. A total of 100 snapshots were recorded during the simulation. The lowest energy conformer of all the complexes was reported as set-1 (Table 2), the highest energy conformer of all the complexes was extracted and reported as set-2 (Table 3), while the docked conformers of

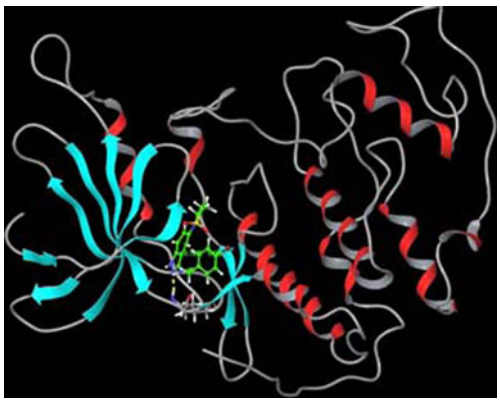

Fig. 1 Binding mode of best inhibitor (compound **14**) within protein cyclin-dependent kinase 2 (CDK2) (1YKR)

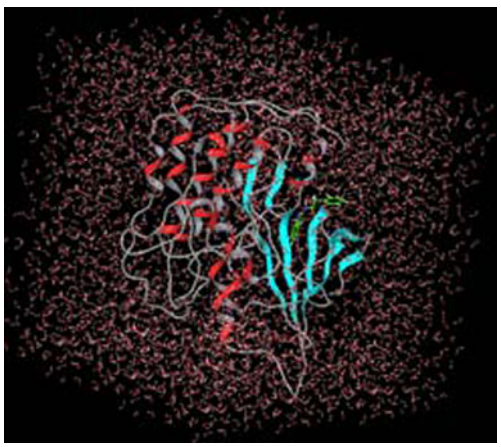

Fig. 2 Protein ligand complex with in solvent [simple point charge (SPC)] water box

Table 2 Quantum mechanics/molecular mechanics (QM/MM)-based descriptor values for low energy conformers with observed and predicted activities

No.	E_{MM}[a]	ΔE_{QM}[b]	η[c]	pIC_{50}	PA_L[d]
1	−55.50789036	0.021094661	0.065365	5.7	7.00
3	−55.65706385	0.040450298	0.07379	6.7	6.34
5	−55.55458129	−5.776841306	0.080005	6.77	6.78
6	−55.41128247	0.036459648	0.078825	5.15	7.77
7	−55.50754096	0.004850376	0.06496	5.7	6.68
8	−55.50357472	0.048338896	0.0788	7.44	7.37
9	−55.43188863	0.026376635	0.074495	8	7.35
12	−55.48993643	−0.009927298	0.0765	8	7.41
13	−55.33217952	0.004521439	0.07395	8	7.79
14	−55.41555693	0.041063169	0.07352	8.15	7.40
15	−55.35129669	−0.004590724	0.074655	8.15	7.70
16	−55.48053026	0.05813479	0.080715	8	7.46
17	−55.42325394	0.01137732	0.08067	8.15	7.72
18	−55.35630045	0.016113403	0.080495	8.05	7.98
19	−55.48616271	−0.012024003	0.082375	7.8	7.41
21	−55.27979196	0.011689252	0.0688	7.4	8.01
23	−55.33726428	−0.010936453	0.06276	8	7.42
24	−55.41983404	0.037401372	0.077445	7.66	7.72
25	−55.41526493	0.017669493	0.06715	7.7	7.40
26	−55.3944685	0.028671866	0.077345	8.05	7.85
2[e]	−55.53339163	0.02238272	0.069735	6.3	6.91
4[e]	−55.64322945	0.016654694	0.071375	5.74	6.43
10[e]	−55.52611792	7.73E-05	0.074375	7.7	6.91
20[e]	−55.36785671	0.033404153	0.06291	8	7.29
27[e]	−55.32627516	0.009946506	0.08254	7.85	8.12
28[e]	−55.13410796	0.020755156	0.06396	7.52	8.35
11[f]	−55.23576776	0.01344789	0.07541	7.62	8.51
22[f]	−55.22110249	0.023160125	0.077355	7.52	8.60

[a]OPLS derived energy of protein with respect to different ligand

[b]Interaction energy of ligand with protein obtained from Eq. 3

[c]Hardness of ligand in bound form obtained from Eq. 4

[d]Predicted activities of low energy conformer based model PA_L

[e]Test set

[f]Outlier compounds

all the complexes, which are more similar to co-crystal ligand, were reported as set-3 (Table 4).

QM/MM methods

All three sets of complexes were subjected to energy calculations. Since determining a DFT description of the whole system would be quite a time-consuming process, ultimately we have used a hybrid QM/MM [21, 22] potential. The ligand energy in bound form was obtained by $QM/MM_{(complex)}$ calculations while the ligand energy in unbound form was obtained by $QM/MM_{(ligand)}$ calculations.

QM/MM (complex)

In $QM/MM_{(complex)}$ analysis we have treated the ligand only with DFT (b3lyp/6–31g* basis set) while the protein and the solvent were described using molecular mechanics (MM) (OPLS2005). The maximum iteration for the geometry optimization was set at 1,000 and a SCF convergence criterion was set as ultrafine ($5*10^{-5}$ Eh) for energy and density matrix convergence ($5*10^{-6}$ RMSD) with a maximum of 1,000 cycles. The convergence accelerator DIIS was used. MM minimization was performed using a maximum 1,000 cycle for criterion of energy convergence ($1*10^{-5}$ Eh) and density matrix convergence ($5*10^{-6}$ RMSD) with conjugate gradient algorithms.

QM/MM (Ligand)

For $QM/MM_{(Ligand)}$ calculations, we used the same conformer of all ligands as those used for $QM/MM_{(complex)}$ analysis in the three geometrical schemes. The ligand was solvated in a 10 Å cubic SPC water box. The energy of the ligand was obtained by QM/MM $_{(Ligand)}$ calculation and in this run the ligand was defined by DFT (b3lyp/6–31g* basis set) while the solvent was described using MM (OPLS2005).

Table 3 QM/MM based descriptor values for high energy conformers with observed and predicted activities

No.	E_{MM}[a]	ΔE_{QM}[b]	η[c]	pIC_{50}	PA_H[d]
1	−56.03219542	0.02484531	0.05474	5.7	6.00
3	−55.7860436	0.023842184	0.068735	6.7	7.66
5	−56.00750116	0.033494581	0.083365	6.77	6.66
6	−55.99435123	0.053270452	0.086485	5.15	6.83
7	−55.99645323	−0.004876906	0.074565	5.7	6.71
8	−55.78383163	0.007644438	0.07702	7.44	7.99
11	−55.873386	0.019417065	0.07577	7.62	7.45
13	−55.83709168	−0.009902669	0.072445	8	7.61
14	−55.78824761	0.031585984	0.07619	8.15	7.80
15	−55.70805502	0.003591277	0.07399	8.15	8.22
16	−55.99509813	0.019063065	0.076635	8	6.78
17	−55.91120207	0.018921105	0.081665	8.15	7.25
18	−55.86749483	0.021439927	0.06958	8.05	7.24
19	−55.86856646	0.025539618	0.07076	7.8	7.17
21	−55.69019055	0.021874827	0.04958	7.4	7.76
22	−55.70576911	0.027909342	0.05784	7.52	7.79
23	−55.73596818	0.013895716	0.064895	8	7.78
24	−55.804791	−0.004034764	0.07766	7.66	7.96
25	−55.72632488	0.018016239	0.05989	7.7	7.76
26	−55.82167311	0.05185236	0.066915	8.05	7.29
2[e]	−56.03256443	0.034175577	0.07265	6.3	6.34
4[e]	−55.90720429	0.008849036	0.06788	5.74	7.11
10[e]	−55.95438914	0.054034798	0.076845	7.7	6.82
20[e]	−55.86612195	0.041772775	0.059145	8	6.89
27[e]	−55.6219439	0.03877626	0.076425	7.85	8.61
28[e]	−55.68058444	0.020135738	0.071165	7.52	8.23
9[f]	−55.55819389	0.020292876	0.07909	8	9.06
12[f]	−56.05361854	0.035299203	0.074465	8	6.17

[a]OPLS derived energy of protein with respect to different ligand

[b]Interaction energy of ligand with protein obtained from Eq. 3

[c]Hardness of ligand in bound form obtained from Eq. 4

[d]Predicted activities of low energy conformer based model PA_H

[e]Test set

[f]Outlier compounds

The remaining protocol for the calculation was same as for the QM/MM $_{(Complex)}$ calculation.

The interaction energy of ligands was obtained using the Eqs. 1–3:

$$E_{QM/MM} = E_{electronic} + E_{nr} + E_{MM} \quad (1)$$

$$E_{Qm} = E_{electronic} + E_{nr} = E_{QM/MM} - E_{MM} \quad (2)$$

$$\Delta E_{\text{int}} = E_{QM(Ligand)} - E_{QM(complex)} \quad (3)$$

The energy of the protein (E_{MM}) was obtained using Eq. 4 and the necessary parameters were obtained from QM/MM $_{(complex)}$ calculations.

$$E_{MM} = E_{QM/MM} - E_{QM} \quad (4)$$

To calculate conceptual DFT properties, we used QM/MM $_{(complex)}$ calculations.

Recently, the absolute hardness η has been defined by Parr et al. [35]

$$\eta = 1/2(\delta\mu/\delta N)_{v(r)} = 1/2\left(\delta^2 E/\delta N^2\right)_{v(r)} \quad (5)$$

Where E is the total energy, N is the number of electrons of the chemical species, and $v(r)$ is the external potential. The operational definition of global hardness can be obtained by finite difference approximation of Eq. 5, which is Eq. 6.

$$\eta = (IP - EA)/2 \quad (6)$$

IP and EA are ionization potential and electron affinity, respectively. According to Koopman's theorem [36], the IP is simply the Eigen value of HOMO with a change of sign, and EA is the Eigen value of LUMO with a change of sign; hence, Eq. 5 may be written as Eq. 6.

$$\eta = (\varepsilon_{LUMO} - \varepsilon_{HOMO})/2 \quad (7)$$

All QM/MM calculations were performed using the QSite [37] interface, which uses the Jaguar [38] program

Table 4 The QM/MM based descriptor values for docked conformers with observed and predicted activities

No.	E_{MM}[a]	ΔE_{QM}[b]	η[c]	pIC_{50}	PA_D[d]
1	−55.60842521	0.02527115	0.067305	5.7	6.36
3	−55.65776985	−967.2545362	0.07777	6.7	6.33
5	−55.62515104	−894.9768511	0.082375	6.77	6.76
6	−55.64627598	−408.9643839	0.08233	5.15	6.50
7	−55.63669169	−358.4452157	0.08265	5.7	6.65
8	−55.60198456	−40.09025454	0.077575	7.44	7.23
9	−55.52006852	59.49052784	0.07887	8	8.35
11	−55.55555745	403.6693173	0.077025	7.62	7.81
12	−55.53452603	323.5891775	0.079155	8	8.23
13	−55.56605364	244.7096449	0.077355	8	7.66
15	−55.51824386	−425.6893018	0.073525	8.15	7.60
16	−55.55141023	−548.498792	0.079715	8	7.90
17	−55.57266704	−114.2262027	0.078635	8.15	7.64
18	−55.57257448	−78.62767702	0.075165	8.05	7.64
19	−55.57164308	−176.799348	0.0679	7.8	6.91
21	−55.37268301	802.534616	0.053575	7.4	8.32
22	−55.38691372	761.1857041	0.051225	7.52	8.04
23	−55.51480692	868.0346797	0.06141	8	7.09
25	−55.5217513	549.9793277	0.067495	7.7	7.65
26	−55.50171368	499.9062873	0.06077	8.05	7.21
2[e]	−55.61312312	−686.5161136	0.072305	6.3	6.33
4[e]	−55.61633728	−889.068495	0.071135	5.74	6.17
10[e]	−55.54399697	23.77803157	0.07733	7.7	8.07
20[e]	−55.48670561	−112.8019644	0.049945	8	6.59
27[e]	−55.41365031	232.6660816	0.071105	7.85	9.18
28[e]	−55.28698166	149.6615516	0.06111	7.52	10.13
14[f]	−55.44536721	−239.969153	0.078515	8.15	9.32
24[f]	−55.45699239	1,023.933292	0.07684	7.66	9.25

[a]OPLS derived energy of protein with respect to different ligand

[b]Interaction energy of ligand with protein obtained from Eq. 3

[c]Hardness of ligand in bound form obtained from Eq. 4

[d]Predicted activities of low energy conformer based model PA_D

[e]Test set

[f]Outlier compounds

for DFT treatment, and the impact [39] program for MM treatment.

CoMFA and CoMSIA

For CoMFA and CoMSIA, the general protocol was the same as described in our earlier publications [26, 27, 40–42]. The molecules were aligned using the same three different geometrical methods as those obtained from MD simulation. The aligned training set of molecules was placed in a 3D grid box such that the entire set was included in the box. Steric and electrostatic (Coulomb potential) field energies were calculated using sp^3 carbon as a probe atom. The energies were truncated to ±30 kcal mol^{-1}. The CoMFA fields generated automatically were scaled by the CoMFA-STD method in SYBYL. CoMSIA was performed using the same lattice box as that used for CoMFA calculations, with a grid spacing of 2.0 Å, employing a C + 1 probe atom with a radius of 1.0 Å as implemented in SYBYL [43].

Regressive validations

The partial least-square (PLS) [44–46] statistical method was used for all 3D QSAR analyses. Column filtering was set as 2.0 kcal mol^{-1} to speed up the analysis and reduce the noise. The CoMFA and CoMSIA descriptors were used as independent variables, and pIC_{50} values were used as dependent variables in PLS regression analyses to derive 3D QSAR models using standard implementation in the SYBYL package. The biological activities were evaluated by the leave-one-out (LOO) cross validation method. The cross-validated correlation coefficient, q^2 and predictive R squared (r^2_{pred}) were calculated using methods described elsewhere [41].

Results

The rules governing the molecular recognition process between a ligand and its receptor (protein) are often

challenging, although hundreds of experimental and computational studies have attempted to quantify them. The available empirical techniques are still insufficient for quantitative descriptions of such interactions. Conformational sampling using molecular docking [47, 48] is often challenged for accuracy. In this context, energy functions and solvent effects can give more insight into binding phenomena. DFT [49] and/or MP2 [50] methods are precise enough to account for such interactions but these calculations remain limited only up to small molecular systems because of the high computational demand. Recently, hybrid potential methods such as QM/MM [21, 22] have been introduced, which can calculate efficiently the properties of macromolecules and can also help with in silico drug discovery [51].

The present study used molecular docking with all complexes solvated using a 55 Å (SPC) water box. A 10 ns MD simulation was performed using protocols described in the Materials and methods section. Afterwards, low energy, high energy, and docked conformers for all complexes were identified and defined as set-1, set-2 and set-3, respectively. QM/MM calculations were performed to calculate the energy and charge density values for all ligands within the protein in its three different conformations.

Energy map

In principal, molecules tend to occupy their lowest energy state. Here, we calculated the total energy of all the ligands in three different conformations using QM/MM methods, followed by application of the equations described above. The molecules were sorted into the lowest and highest energy sets using the total energy (QM/MM) of the complex, while docked conformers were taken directly from the molecular docking information, which is the same as the starting structure for MD simulations. Interestingly, we found that, in all cases, the ligand QM energy was minimum in the docked conformation. This indicates that the ligand achieves maximum stability in the docked conformation and this is a good indication to set an additional docking score. As a consequence, we calculated the interaction energy ΔE_{int} using QM/MM $_{(complex)}$ and QM/MM $_{(Ligand)}$ calculations as described in Materials and methods. The values of interaction energy ΔE_{int} are reported under Tables 2, 3, 4 for sets 1–3, respectively.

Quantum chemical properties and activity relationships

The interaction energies of ligands to the receptor (ΔE_{int}) were calculated using QM/MM techniques as described in Eqs. 1–3. The frontier orbital energies (ε_{HOMO}, ε_{LUMO}) and charge densities were used to evaluate important conceptual DFT-based parameters such as global hardness (η) [52] electronegativity (χ) [53], chemical potential (μ) [54] and electrophilicity index (ω) [55], etc. These important descriptors were related as a function of variation of biological activities using multiple linear regression analysis. The correlation matrix was developed using a collinear cutoff of 0.5, and all linearly related descriptor were removed physically from the analyses with only the best and most significant models presented here. For the first set, we derived a model PA_L (predicted activity for low energy conformer) that includes the interaction energy of the ligand to the protein ΔEint, global hardness (η) and receptor energy E_{MM}.

Model PA_L

Variable	Coefficient	SE	T
Intercept	2.4937e+02	1.3458e+02	1.8530
E_{MM}	4.4070e+00	2.4308e+00	1.8130
ΔE_{int}	6.3969e−02	1.6712e−01	0.3828
η	3.2338e+01	3.0730e+01	1.0523

SD=0.88, R^2=0.22, F=1.6, q^2=0.02, RMS=7.49

The model has a relationship with biological activities, as is clear from the correlation coefficient r^2=0.22 for the training set, but the cross validated correlation coefficient q^2 was too low to be considered significant.

For the second set, we derived a model PA_H (predicted activity for high energy conformer) using the same descriptors as those as for the previous model PA_L.

Model PA_H

Variable	Coefficient	SE	T
Intercept	2.9570e+02	9.7157e+01	3.0435
E_{MM}	5.1865e+00	1.7481e+00	2.9670
ΔE_{int}	−7.1142e+00	1.1905e+01	0.5976
η	2.0829e+01	1.8049e+01	1.1540

SD=0.7, R^2=0.38, F=3.3, q^2=0.03, RMS=0.94

This model has a good relationship, with a value of correlation coefficient r^2=0.38 for the training set but the cross-validated correlation coefficient q^2 still remains poor.

Finally, we derived a model PA_D (predicted activity for docked conformer). The descriptors were same as for the previous models. The model PA_D showed good correlation with biological activity. The correlation coefficient r^2=0.50 for the training set and the cross validated correlation coefficient (q^2) was 0.26.

Model PA_D

Variable	Coefficient	SE	T
Intercept	7.8101e+02	2.3359e+02	3.3435
E_{MM}	1.4021e+01	4.2269e+00	3.3172
ΔE_{int}	5.4140e−05	4.7345e−04	0.1144
η	7.2465e+01	2.6962e+01	2.6877

SD=0.7, R^2=0.50, F=5.4, q^2=0.26, RMS=0.8

The descriptors that provided a good relationship are conceptually valid as the interaction energy ΔE_{int} is a fundamental parameter for the activity. In QM/MM calculations, the interaction energy was concerned mainly with the energy of the ligand (QM energy) and the variation of protein energy with respect to different ligands, which is considered an important parameter, was missing. Eventually, the inclusion of receptor energy (E_{MM}) gave a good relationship with the variation of activity. According to the maximum hardness principle [52], the molecule gains maximum hardness in its most stable form. The noteworthy finding in all cases was that the global hardness had a positive coefficient, indicating a high hardness value as a favorable parameter for biological activity, which means a stable complex will have higher inhibitory activity.

For these three models, the best statistics (q^2=0.26, r^2= 0.50) were associated with the docked conformer based model PA_D. The predicted and observed biological activities for all the models along with the descriptor values are given in Tables 2, 3, 4.

Comparative three-dimensional analysis

Three-dimensional analyses were performed using the aforementioned three different geometrical schemes, namely low energy, high energy and docked conformer, respectively.

Frontier orbital density map

The electron density distribution is a function of conformation, which plays an important role in drug receptor interactions. The HOMO density maps drawn for all three conformers are shown in Fig. 3a–c.

The maps in Fig. 3a and b correspond to the low and high-energy conformers with high HOMO density around indazole ring. In the case of the docked conformer (Fig. 3c), high HOMO density is located around the phenyl ring with no HOMO density around the sulfur, oxygen or indazole ring. This map indicates a possible steric and bulk interaction rather than an electrostatic interaction around SO_2 and the indazole ring. This map provides a very useful demonstration of the variation of electron density due to slight conformational changes in the ligand or its surrounding residues. Such small variations in conformation effectively perturb the nature of the resulting interaction.

Electrostatic potential and electron density

The charge and electron density maps for different conformers of the most active molecule (compound **14**), as determined by the DFT/MM method, are illustrated in Fig. 4a–c.

The differences between these three electron density maps gave a direct indication of charge migration due to polarization. Therefore, we could determine the change in the electron density and electrostatic potential of each inhibitor for different conformations within the protein. The electron density (cage) and electrostatic potential (surface) maps for representative structures are shown in Fig. 4. As we can see in Fig. 4a and c, the electrostatic potential distribution is similar (bluish in color) and the potential ranges were set as 43 and 45 kcal mol^{-1}, while the map in Fig. 4b (high energy conformer) is red in color, which indicates a rather negative potential; the range was set as 49 kcal mol^{-1}. The electron density maps were similar in all three conformations except for the zone between SO_2 and the carbonyl oxygen atom. This particular zone was most neutral in docked conformation as shown by the white surface in Fig. 4c. Even though both the oxygen atoms have lone pair of electrons and the sulfur atom also has a lone pair of electrons, the low electron density around these region indicates that their bulk might contribute to a steric interaction rather than an electrostatic one.

Molecular alignment

Molecular alignment is a key step in comparative molecular field analyses (CoMFA). In this study, the molecules were aligned in each case, using a common sub-structure based method and the most active molecule (compound **14**) was used as template in its three different conformations (high energy, docked and low energy) for respective geometrical schemes. The docked geometry based molecular alignment is displayed in Fig. 5.

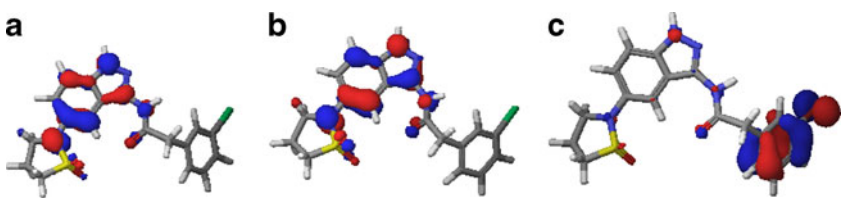

Fig. 3 HOMO density map for **a** lowest energy conformer, **b** highest energy conformer, **c** docked conformer for ligand **14**

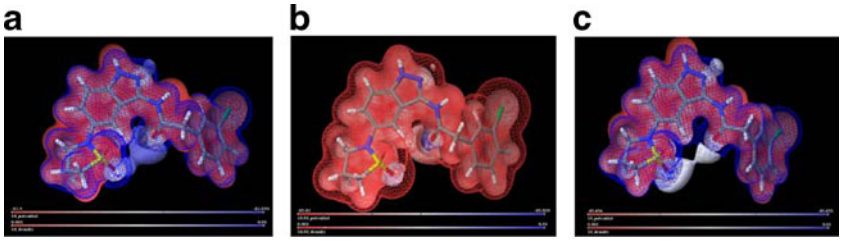

Fig. 4 Electron density (*solid surface*) and electrostatics potential (*mesh*) density map for **a** lowest energy conformer, **b** highest energy conformer, **c** docked conformer for the ligand **14**

Comparative molecular fields analyses

The CoMFA model was developed using the same training and test sets as those for QM/MM based models. The molecular charges were assigned using the Gasteiger-Hückel method. The steric "S", electrostatic "E" and both fields together were used to develop three different models for each geometrical scheme (a total of nine models: $CoMFA_1$–$CoMFA_9$). Models $CoMFA_1$–$CoMFA_3$ were based on the low energy conformer; models $CoMFA_4$–$CoMFA_6$ were based on the high-energy conformer, while models $CoMFA_7$–$CoMFA_9$ were based on the docked conformer.

In both the low energy and high energy conformer-based models, the electrostatic field alone showed significant relationships ($CoMFA_2$ q^2=0.32 and $CoMFA_5$ q^2=0.31) with the variation in inhibitory activity. Model 3 ($CoMFA_3$) was based on both fields having values LOO q^2=0.22 and r^2=0.59. $Model_6$ ($CoMFA_6$) was based on both fields having values LOO q^2=0.23 and r^2=0.55. Similarly the $model_9$ ($CoMFA_9$) was based on both fields having values LOO q^2=0.50 and r^2=0.71.

Of the three steric field-based models ($CoMFA_1$, $CoMFA_4$ and $CoMFA_7$) the docked conformer based steric model ($CoMFA_7$) has the better relationship (q^2=0.49). It is evident that the docked geometry is important in accounting for the interactions. In the docked-geometry-based models, $CoMFA_9$ showed a significant relationship. Even though this model involves both steric and electrostatic interactions, the electrostatic contribution was observed to be dominant for the interaction. The model successfully showed a valid internal predictivity value $r^2_{bs} = 0.72$] and for predictivity of the six molecules of the test set the $r^2_{predictive}$ value was 0.66. This is more realistic because it is based on the co-crystallized binding mode, all molecules have nearly the same conformation as the co-crystal structure, and all have key contact hydrogen bonding between residues Glu81, Leu83, etc. The statistical summary of all nine models is presented in Table 5. The activities predicted by CoMFA are summarized in Table 7. The trends of observed and predicted activities using model $CoMFA_9$ are displayed in Fig. 6.

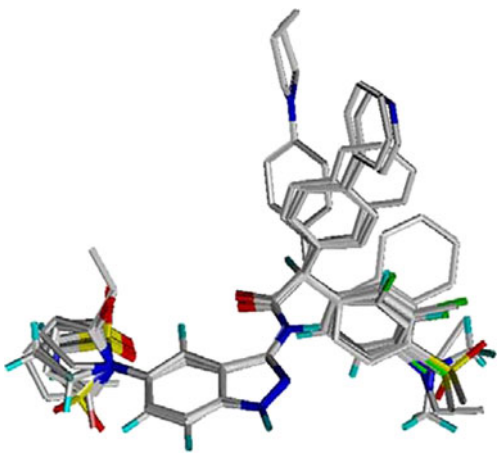

Fig. 5 Docked alignment over co-crystal ligand **14**

CoMFA maps

The 3D-CoMFA contour map using the best-fit model $CoMFA_9$ is displayed in Fig. 7 to demonstrate the comparative molecular field effects over compound **14**.

In Fig. 7 the green contour indicates the area in which bulky substations might affect the activity beneficially, and the yellow region is favorable for small groups. The blue contour (Fig. 7) indicates the region where a positive group will be helpful for high activity, while the red zone indicates the region favorable for negative groups. The green and blue contours were evident around isothiazolidine, indicating that a bulkier and/or positive group around these regions will favor high activity. Yellow contours were evident just near indazole and around the SO_2 group of isothiazolidine, indicating that a small group will be favored around these regions for higher activity.

Comparative molecular similarity indices analyses

Comparative molecular similarity indices analyses (CoMSIA) was conducted in a manner similar to CoMFA with the protocol described in the Materials and methods section. CoMSIA was conducted using steric and electrostatic fields effects separately as well as jointly for all three geometrical schemes as noted in Table 6. In the case of the low-energy- and high-energy-

Table 5 Regression summary of different comparative molecular fields analyses (CoMFA) models. Fields: *S* Steric, *E* electrostatic

No.	Model	Field	q^2	n	r^2	SE	F	$r^2_{observed}$	SD	$r^2_{predicted}$
Low energy conformer based										
1	CoMFA1	S	−0.667	3	0.869	0.346	39.727	–	–	–
2	CoMFA2	E	0.32	1	0.578	0.588	27.397	–	–	–
3	CoMFA3	0.45S/0.55E	0.22	1	0.59	0.577	29.313	–	–	–
High energy conformer based										
4	CoMFA4	S	−0.331	3	0.863	0.353	37.831	–	–	–
5	CoMFA5	E	0.31	1	0.549	0.608	24.345	–	–	–
6	CoMFA6	0.44S/0.56E	0.23	1	0.55	0.606	24.719	–	–	–
Docked conformer based										
7	CoMFA7	S	0.49	1	0.753	0.45	61.082	–	–	–
8	CoMFA8	E	0.46	1	0.672	0.51	40.964	–	–	–
9	CoMFA9	0.49S/0.51E	0.50	1	0.71	0.49	48.04	0.72	0.11	0.66

based models, the electrostatic field alone is better than the steric field effect-based models.

The low energy based electrostatic model ($CoMSIA_2$) has LOO q^2=0.68 while the high energy based electrostatic model ($CoMSIA_5$) has LOO q^2=0.65. The steric field based models $CoMSIA_1$ and $CoMSIA_4$ have a poor relationship with activity, but with the docked geometry based model there is a significant change; the steric field based model ($CoMSIA_7$) has q^2 0.30 and the model $CoMSIA_9$, which uses both steric and electrostatic fields effects, has q^2 0.60 and a correlation coefficient of r^2=0.86. The X-ray geometry based best-fit model $CoMSIA_9$ with the steric and electrostatic field effects, was tested for internal predictive power ($r^2_{bs} = 0.90$) and for the test set predictive power of six compounds ($r^2_{predictive} = 0.55$). The statistical value for model $CoMSIA_9$ was better among other models, which indicates the significance of docked geometry to account for the steric contribution to inhibitory activity. However, in all three geometrical schemes, the electrostatic contribution was dominant. The different field combinations and the statistical summary are reported in Table 6. The predicted activities using model $CoMSIA_9$ are presented in Table 7 and the trend of observed and predicted activities using model $CoMSIA_9$ is displayed in Fig. 8.

CoMSIA maps

Like CoMFA, the CoMSIA contour maps were developed using the docking-based CoMSIA model. The model was based on steric and electrostatic field effects. Each field effect is displayed individually in Fig. 9 over compound **14**.

The green contours (Fig. 9) indicate the area in which bulky substitutions might affect the activity beneficially, and the yellow region is favorable for small groups. The map is quite similar to the CoMFA steric map as the green and blue contour appears around isothiazolidine, which indicates that a bulkier/positive group will be favorable for higher activity. There is a yellow contour around the phenyl group, which is directed towards residues Ile10, Gle85 and His84, and these

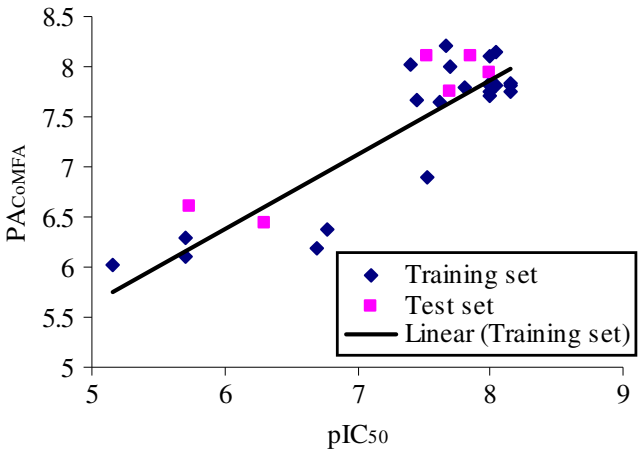

Fig. 6 Trend of observed and predicted activities for the training and test set using CoMFA based model ($CoMFA_9$)

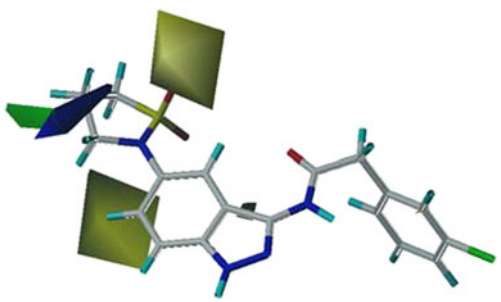

Fig. 7 CoMFA steric and electrostatic maps based on $model_9$ ($CoMFA_9$)

Table 6 Regression summary of different comparative molecular similarity indices analyses (CoMSIA) models

Model	Field	q^2	n	r^2	SE	F	$r^2_{observed}$	SD	$r^2_{predicted}$
Low conformer based									
CoMSIA1	S	−0.799	2	0.469	0.677	8.375	–	–	–
CoMSIA2	E	0.68	2	0.809	0.406	40.334	–	–	–
CoMSIA3	0.148S/0.852E	0.591	2	0.82	0.388	45.124	–	–	–
High conformer based									
CoMSIA4	S	−0.363	2	0.243	0.809	3.046	–	–	–
CoMSIA5	E	0.65	2	0.798	0.417	37.615	–	–	–
CoMSIA6	0.11S/0.89E	0.53	2	0.78	0.43	34.57	–	–	–
Docked conformer based									
CoMSIA7	S	0.30	2	0.646	0.553	17.301	–	–	–
CoMSIA8	E	0.574	2	0.875	0.329	66.315	–	–	–
CoMSIA9	0.22S/0.78E	0.60	2	0.86	0.34	59.62	0.90	0.05	0.55

residues are all within the 3 Å range, which indicates a suitable site for a small substituent.

Table 7 Observed (reference) and predicted activities by CoMFA and CoMSIA models

No.	pIC_{50}	PA_{COMFA9}	Residue	$PA_{CoMSIA9}$	Residue
1	5.7	6.1	−0.4	5.8	−0.1
3	6.7	6.19	0.51	6.42	0.28
5	6.77	6.38	0.39	6.06	0.71
6	5.15	6.02	−0.87	5.95	−0.80
7	5.7	6.29	−0.59	5.79	−0.09
8	7.44	7.67	−0.23	7.72	−0.28
9	8	7.71	0.29	8.03	−0.03
11	7.62	7.65	−0.03	7.84	−0.22
12	8	7.75	0.25	7.91	0.09
13	8	7.83	0.17	7.91	0.09
14	8.15	7.75	0.4	7.87	0.28
15	8.15	7.82	0.33	7.86	0.29
16	8	7.82	0.18	7.77	0.23
17	8.15	7.84	0.31	7.73	0.42
18	8.05	7.81	0.24	7.87	0.18
19	7.8	7.8	0	7.81	−0.01
21	7.4	8.03	−0.63	7.76	−0.36
22	7.52	6.9	0.62	7.51	0.01
23	8	8.1	−0.1	7.83	0.17
24	7.66	8.2	−0.54	7.96	−0.30
25	7.7	8.01	−0.31	7.78	−0.08
26	8.05	8.14	−0.09	8.46	−0.41
Test set					
2	6.3	6.43	−0.13	6.09	0.21
4	5.74	6.6	−0.86	6.53	−0.79
10	7.7	7.76	−0.06	7.98	−0.28
20	8	7.94	0.06	7.81	0.19
27	7.85	8.11	−0.26	8.47	−0.62
28	7.52	8.11	−0.59	8.46	−0.94

Discussion

In general, stable molecular systems tend to have minimum energy. In ligand receptor–interaction studies such information is needed to analyze the stability of ligands when present in the complex. According to the maximum hardness principal [52] the molecule must gain maximum hardness value for stability. The conceptual phenomena for these two parameters are illustrated in Scheme 1.

In our analysis, we noted the minimum energy for the ligands (E_{QM}) in docked conformation. The positive coefficient of ΔE_{int} and the hardness indicate that a high hardness value and high interaction energy favor inhibitory activity against CDK2.

It is expected that the use of QM methods will keep growing in all phases of computer-aided drug design and development. However, extensive sampling of conformational space and treatment of solution of macromolecules

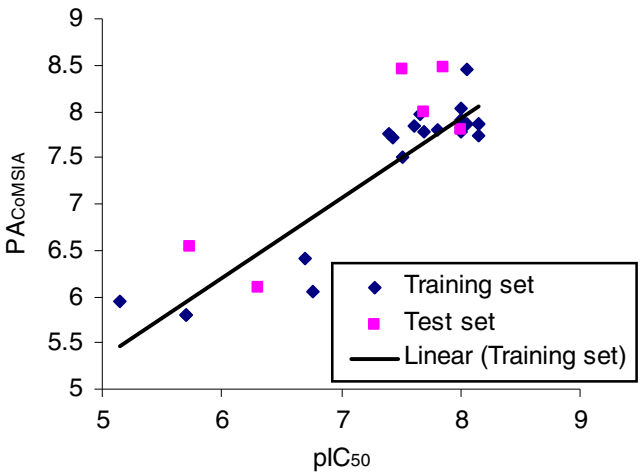

Fig. 8 Trend of observed and predicted activities for the training and test set using CoMSIA based model ($CoMSIA_9$)

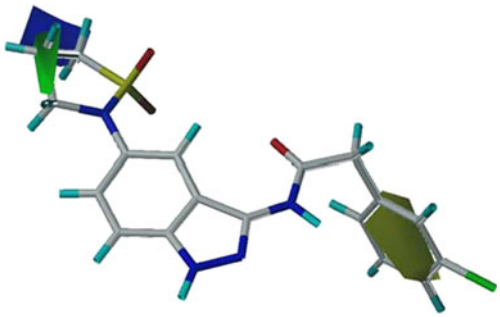

Fig. 9 CoMSIA steric and electrostatic map based on model $CoMSIA_9$

are still a limiting factor for the broad application of QM in drug design. To overcome these limitations, and in order to account for steric and bulk interactions, we used the well-established CoMFA and CoMSIA methods.

Conclusions

There continues to be some debate surrounding bioactive conformers. In ligand-based design, the lowest energy conformer has often been considered as the most bioactive conformer: however, in structure-based design, molecular docking remains the ultimate choice. Here, we find that the low energy conformer provided a better description of the electronic and electrostatic interaction but that steric and van der Waals interactions remained poorly defined in such studies. A combined approach using steric and electrostatic interactions gave more insight. The slight variation in the conformation might perturb the electron density distribution and electrostatic potential, which might lead to a different interaction. Comparing ligand interaction energy is helpful in identifying bioactive conformers among different conformational samples. The low energy and high hardness based conformer is thought to be the bioactive conformer. In spite of a good statistical relationship we cannot overlook the contribution of other interactions; deep analyses and consideration of steric interactions supports docking-based conformers.

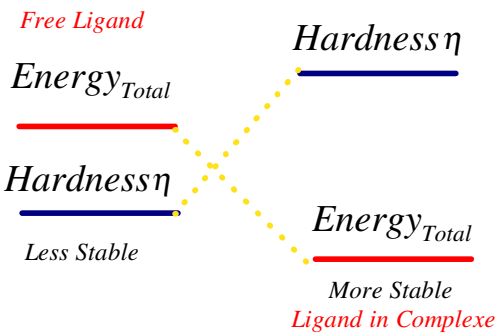

Scheme 1 Conceptual assumptions of energy and hardness

CoMFA and CoMSIA indicated that bulkier and/or positive groups around the indazole group and a small group around the SO_2 group of isothiazolidine will be helpful for better activity of CDK2 inhibitors. Finally, we conclude that more sophisticated techniques such as DFT-based electronic energy calculations, QM/MM and molecular dynamics have limitations. There is a need to account for the various kinds of interactions to access biological activities in computational drug design.

References

1. Sausville EA, Johnson J, Alley M, Zaharevitz D, Senderowicz AM (2000) Inhibition of CDKs as a therapeutic modality. Ann N Y Acad Sci 910:207–222
2. Kaldis P (1999) The cdk-activating kinase (CAK): from yeast to mammals. Cell Mol Life Sci 55:284–296
3. Gu Y, Rosenblatt J, Morgan DO (1992) Cell-cycle regulation of Cdk2 activity by phosphorylation of Thr160 and Tyr15. EMBO J 11:3995–4005
4. Solomon MJ, Lee T, Kirschner MW (1992) Role of phosphorylation in P34cdc2 activation—identification of an activating kinase. Mol Biol Cell 3:13–27
5. Matsuoka M, Kato JY, Fisher RP, Morgan DO, Sherr CJ (1994) Activation of cyclin-dependent Kinase-4 (Cdk4) by mouse Mo15-associated kinase. Mol Cell Biol 14:7265–7275
6. Hagopian JC, Kirtley MP, Stevenson LM, Gergis RM, Russo AA, Pavletich NP, Parsons SM, Lew J (2001) Kinetic basis for activation of CDK2/clyclin A by phosphorylation. J Biol Chem 276:275–280
7. Ducommun B, Brambilla P, Felix MA, Franza BR, Karsenti E, Draetta G (1991) Cdc2 phosphorylation is required for its interaction with cyclin. EMBO J 10:3311–3319
8. Desai D, Wessling HC, Fisher RP, Morgan DO (1995) Effects of phosphorylation by Cak on cyclin binding by Cdc2 and Cdk2. Mol Cell Biol 15:345–350
9. Gartel AL, Tyner AL (2002) The role of the cyclin-dependent kinase inhibitor p21 in apoptosis. Mol Cancer Ther 1:639–649
10. Dulic V, Lees E, Reed SI (1992) Association of human Cyclin-E with a periodic G(1)-S phase protein-kinase. Science 257:1958–1961
11. Koff A, Giordano A, Desai D, Yamashita K, Harper JW, Elledge S, Nishimoto T, Morgan DO, Franza BR, Roberts JM (1992) Formation and activation of a Cyclin E-Cdk2 complex during the G(1)-phase of the human cell-cycle. Science 257:1689–1694
12. Hinds PW, Mittnacht S, Dulic V, Arnold A, Reed SI, Weinberg RA (1992) Regulation of retinoblastoma protein functions by ectopic expression of human cyclins. Cell 70:993–1006
13. Hatakeyama M, Brill JA, Fink GR, Weinberg RA (1994) Collaboration of G(1) cyclins in the functional inactivation of the retinoblastoma protein. Genes Dev 8:1759–1771
14. Cardoso MC, Leonhardt H, Nadalginard B (1993) Reversal of terminal differentiation and control of DNA-replication - Cyclin-a and Cdk2 specifically localize at subnuclear sites of DNA-replication. Cell 74:979–992
15. Vandenheuvel S, Harlow E (1993) Distinct roles for cyclin-dependent kinases in cell-cycle control. Science 262:2050–2054
16. Ishimi Y, Komamura-Kohno Y, You ZY, Omori A, Kitagawa M (2000) Inhibition of Mcm4,6,7 helicase activity by phosphorylation with cyclin A/Cdk2. J Biol Chem 275:16235–16241

17. Sherr CJ (2000) The Pezcoller lecture: cancer cell cycles revisited. Cancer Res 60:3689–3695
18. Davies TG, Pratt DJ, Endicott JA, Johnson LN, Noble MEM (2002) Structure-based design of cyclin-dependent kinase inhibitors. In: Proceedings of pharmacology and therapeutics: 2nd international conference on inhibitors of protein kinases, vol 93. Elseview, Amsterdam, pp 125–133
19. Wyatt PG, Woodhead AJ, Berdini V, Boulstridge JA, Carr MG, Cross DM, Davis DJ, Devine LA, Early TR, Feltell RE, Lewis EJ, McMenamin RL, Navarro EF, O'Brien MA, O'Reilly M, Reule M, Saxty G, Seavers LCA, Smith DM, Squires MS, Trewartha G, Walker MT, Woolford AJA (2008) Identification of N-(4-piperidinyl)-4-(2,6-dichlorobenzoylamino)-1 H-pyrazole-3-carboxamide (AT7519), a novel cyclin dependent kinase inhibitor using fragment-based X-ray crystallography and structure based drug design. J Med Chem 51:4986–4999
20. Pople JA, Gill PMW, Johnson BG (1992) Kohn-Sham density-functional theory within a finite basis set. Chem Phys Lett 199:557–560
21. Field MJ, Bash PA, Karplus M (1990) A combined quantum-mechanical and molecular mechanical potential for molecular-dynamics simulations. J Comput Chem 11:700–733
22. Warshel A, Levitt M (1976) Theoretical studies of enzymic reactions—dielectric, electrostatic and steric stabilization of carbonium-ion in reaction of lysozyme. J Mol Biol 103:227–249
23. Jorgensen WL, Tiradorives J (1988) The Opls potential functions for proteins—energy minimizations for crystals of cyclic-peptides and crambin. J Am Chem Soc 110:1657–1666
24. Singh PP, Pasha FA, Srivastava HK (2004) Novel application of softness parameter for regioselectivity and reaction mechanism. Ind J Chem B 43:983–991
25. Singh PP, Srivastava HK, Pasha FA (2004) DFT-based QSAR study of testosterone and its derivatives. Bioorg Med Chem 12:171–177
26. Pasha FA, Chung HW, Kang SB, Cho SJ (2008) 3D-quantitative structure activity analysis and quantum chemical analysis of pyrido-di-indoles. Int J Quantum Chem 108:391–400
27. Pasha FA, Dal Nam K, Cho SJ (2007) CoMFA based quantitative structure toxicity relationship of azo dyes. Mol Cell Toxicol 3:145–149
28. Cramer RD, Patterson DE, Bunce JD (1988) Comparative molecular-field analysis (Comfa). 1. Effect of shape on binding of steroids to carrier proteins. J Am Chem Soc 110:5959–5967
29. Klebe G (1994) The use of composite crystal-field environments in molecular recognition and the de novo design of protein ligands. J Mol Biol 237:212–235
30. Klebe G, Abraham U, Mietzner T (1994) Molecular similarity indexes in a comparative-analysis (Comsia) of drug molecules to correlate and predict their biological-activity. J Med Chem 37:4130–4146
31. Lee J, Choi H, Kim KH, Jeong S, Park JW, Baek CS, Lee SH (2008) Synthesis and biological evaluation of 3,5-diaminoindazoles as cyclin-dependent kinase inhibitors. Bioorg Med Chem Lett 18:2292–2295
32. Glide (2005) User's Guide, version 4.0, Schrödinger, LLC, New York, NY
33. Maestro (2006) User's guide, version 7.5, Schrödinger, LLC, New York, NY
34. Hamdouchi C, Zhong B, Mendoza J, Collins E, Jaramillo C, De Diego JE, Robertson D, Spencer CD, Anderson BD, Watkins SA, Zhang F, Brooks HB (2005) Structure-based design of a new class of highly selective aminoimidazo [1, 2-a] pyridine-based inhibitors of cyclin dependent kinases. Bioorg Med Chem Lett 15:1943–1947
35. Parr RG, Pearson RG (1983) Absolute hardness—companion parameter to absolute electronegativity. J Am Chem Soc 105:7512–7522
36. Koopmans T (1933) Ordering of wave functions and eigenenergies to the individual electrons of an atom. Physica 1:104–113
37. QSite (2005) User's guide, ver 4.0, Schrödinger, LLC, New York, NY
38. Jaguar (2007) User's guide, ver 6.5, Schrödinger, LLC, New York, NY
39. MacroModel (2005) User's guide, ver 9.1, Schrödinger, LLC, New York, NY
40. Pasha FA, Muddassar M, Beg Y, Cho SJ (2008) DFT-based de novo QSAR of phenoloxidase inhibitors. Chem Biol Drug Des 71:483–493
41. Pasha FA, Muddassar M, Neaz MM, Cho SJ (2009) Pharmacophore and docking-based combined in-silico study of KDR inhibitors. J Mol Graph Model 28:54–61
42. Pasha FA, Neaz MM, Cho SJ, Kang SB (2007) Quantitative structure activity relationship (QSAR) study of estrogen derivatives based on descriptors of energy and softness. Chem Biol Drug Des 70:520–529
43. Tripos (2007) Sybyl 7.3, Tripos International; St. Louis, MO
44. Geladi P, Xie YL, Polissar A, Hopke P (1998) Regression on parameters from three way decomposition. J Chemom 2:231
45. Wold S (1978) Cross-validatory estimation of number of components in factor and principal components models. Technometrics 20:397–405
46. Wold S, Ruhe A, Wold H, Dunn WJ (1984) The collinearity problem in linear-regression—the Partial Least-Squares (Pls) approach to generalized inverses. JoSIAM J Sci Stat Computurnal 5:735–743
47. Lengauer T, Rarey M (1996) Computational methods for biomolecular docking. Curr Opin Struct Biol 6:402–406
48. Sandak B, Nussinov R, Wolfson HJ (1998) A method for biomolecular structural recognition and docking allowing conformational flexibility. J Comput Biol 5:631–654
49. Zhou T, Huang DZ, Caflisch A (2010) Quantum mechanical methods for drug design. Curr Top Med Chem 10:33–45
50. Møller C, Plesset MS (1934) Note on an approximate treatment for many–electron systems. Phys Rev 46:618–622
51. Yang WT, Parr RG (1985) Hardness, softness, and the fukui function in the electronic theory of metals and catalysis. Proc Natl Acad Sci USA 82:6723–6726
52. Parr RG, Chattaraj PK (1991) Principle of maximum hardness. J Am Chem Soc 113:1854–1855
53. Parr RG, Von Szentpaly L, Liu SB (1999) Electrophilicity index. J Am Chem Soc 121:1922–1924
54. Parr RG, Donnelly RA, Levy M, Palke WE (1978) Electronegativity—density functional viewpoint. J Chem Phys 68:3801–3807
55. Chattaraj PK, Maiti B, Sarkar U (2003) Philicity: a unified treatment of chemical reactivity and selectivity. J Phys Chem A 107:4973–4975